Research article

Wancai Li, Jiaqi Ma, Haizhen Wang, Chen Fang, Hongmei Luo and Dehui Li*

Biexcitons in 2D (iso-BA)$_2$PbI$_4$ perovskite crystals

https://doi.org/10.1515/nanoph-2019-0528
Received December 17, 2019; revised January 15, 2020; accepted January 26, 2020

Abstract: Two-dimensional (2D) organic-inorganic hybrid perovskites have attracted growing attention recently due to their naturally formed quantum-well structure, unique photoelectric properties and better environmental stability compared to three-dimensional perovskites. The reduced screening and enhanced Coulomb interaction in 2D perovskites result in the formation of excitonic complexes. While the properties of free excitons have been well investigated, studies on biexcitons remain elusive. Here, we report on the biexcitons in 2D (iso-BA)$_2$PbI$_4$ (BA=$C_4H_9NH_3$) crystals. The biexciton emission can be observed under a very low excitation power density of 6.4 W/cm^2 at 78 K. The biexciton exhibits a large biexciton binding energy of 46 meV due to the large exciton binding energy of (iso-BA)$_2$PbI$_4$. Furthermore, the biexcitons exhibit a favorable polarization orientation, resulting in different anisotropy between biexcitons and excitons. Our findings would motivate more studies on biexcitons in 2D perovskites and pave the way for exploiting the many-body physics for biexciton lasing and optical storage devices.

Keywords: biexcitons; quantum wells; optical anisotropy; 2D perovskites.

1 Introduction

Two-dimensional (2D) organic-inorganic hybrid perovskites exhibit unique optical properties due to their naturally formed quantum well-structure and layered nature [1]. Due to the Coulomb interaction binding electrons and holes, quasi-particles named excitons are formed. The significant difference in dielectric constant between the organic barrier layers and the inorganic well layers leads to the enhanced Coulomb interaction in the well layers, resulting in the extreme large exciton binding energy in 2D perovskites [2, 3]. If the exciton binding energy is larger than the thermal excitation energy, excitons cannot be thermally ionized. We can observe the exciton emission spectrum in perovskites since excitons have a lower energy than free carriers [4–6]. As a consequence, a series of novel optical properties, such as the formation of excitonic complexes, are present in 2D perovskites, which make 2D perovskites attractive for potential exciton-related applications [7, 8].

Biexciton, formed by binding two excitons together, has been studied in 2D transition metal dichalcogenides such as WSe_2 [9–11] and 2D organic-inorganic hybrid perovskites such as $(C_4H_9NH_3)_2PbBr_4$ and $(C_{10}H_{21}NH_3)_2PbI_4$ crystals [12, 13]. Strong many-body Coulomb interactions lead to the emergence of biexcitons, forming a bound state with a lower energy than free excitons, which can be reflected in the PL spectra. The enhancement of the quantum confinement in structures of reduced dimensionality such as quantum wells, wires and dots results in the formation of the excitonic complexes. Biexcitons have important applications in lasing due to the reduced self-absorption effect compared to conventional excitonic lasing [14]. Generally, high excitation power density and low temperature (e.g. 4 K) are required to observe the biexciton emission since biexciton emission essentially is a nonlinear process [15]. Therefore, it is necessary to explore new materials for the biexciton emission with a low excitation power density for biexciton-associated optoelectronic applications.

Here, we report the biexciton emission in 2D perovskite (iso-BA)$_2$PbI$_4$ (BA=$C_4H_9NH_3$) crystals at liquid nitrogen temperature by temperature- and power-dependent photoluminescence (PL) spectroscopy. The excitation power density of the biexcitons is below 6.4 W/cm^2, due to the enhanced Coulomb interaction and the reduced screening effect. A large biexciton binding energy of 46 meV has been observed due to the large exciton binding energy

***Corresponding author: Dehui Li,** School of Optical and Electronic Information and Wuhan National Laboratory for Optoelectronics, Huazhong University of Science and Technology, Wuhan 430074, China, e-mail: dehuili@hust.edu.cn. https://orcid.org/0000-0002-5945-220X
Wancai Li, Jiaqi Ma and Chen Fang: School of Optical and Electronic Information, Huazhong University of Science and Technology, Wuhan 430074, China
Haizhen Wang and Hongmei Luo: Department of Chemical and Materials Engineering, New Mexico State University, Las Cruces, NM 88003, USA

in (iso-BA)$_2$PbI$_4$ crystals. In addition, biexcitons exhibit a rather different anisotropy compared to that of excitons. The study of power dependence and anisotropy of biexcitons is beneficial to the further understanding of biexcitons, which has important applications of novel photoelectric detectors, solar cells and biexciton lasing [14, 16–20].

2 Experiments

2.1 Sample preparation

The synthesis of the (iso-BA)$_2$PbI$_4$ and (n-BA)$_2$PbI$_4$ perovskites can be found in our previous reports [21, 22]. Perovskite microplates were directly exfoliated from their respective bulk crystals onto a pre-cleaned 300 nm SiO_2/Si substrate by using Scotch tape.

2.2 Material characterizations

Atomic force microscope image and scanning electron microscope (SEM) image were taken on a Bruker Dimension EDGE microscopy and a Tescan Vega3 microscopy, respectively. The PL spectra were acquired in a confocal micro-Raman system (Horiba HR550) equipped with a 600 g mm^{-1} grating in a backscattering configuration excited by a 405-nm solid-state laser. For the low-temperature measurement, we used a liquid nitrogen continuous-flow cryostat (Cryo Industry of America, USA) to control the temperature from 78 K to 290 K at a base pressure of 10^{-6} mBar evacuated by a molecular pump.

3 Results

Figure 1A displays the crystal structure of (iso-BA)$_2$PbI$_4$, which is comprised by the corner-sharing PbI$_4$ octahedrons with iso-BA$^+$ ions filling between layers. iso-BA$^+$ is the short branched chain butylamine (iso-BA) spacer cation, which is the isomer of n-BA [23, 24]. The (iso-BA)$_2$PbI$_4$ bulk crystals are synthesized according to the previously reported method [25]. To investigate their optical properties, the (iso-BA)$_2$PbI$_4$ microplates are obtained by mechanically exfoliated from as-synthesized bulk crystals. The optical microscope images and SEM images of the as-prepared (iso-BA)$_2$PbI$_4$ microplates reveal that those microplates have rather smooth surface and are tens of micrometers in width and length (Figure 1B and C). Since iso-BA is the isomer of n-BA, the PL spectra of (iso-BA)$_2$PbI$_4$ and (n-BA)$_2$PbI$_4$ are similar at 290 K (Figure S1A and B). Nevertheless, (n-BA)$_2$PbI$_4$ shows a phase transition at low temperature while there is no such phase transition for (iso-BA)$_2$PbI$_4$ at low temperature [26]. In particular, two emission peaks are also observed for (iso-BA)$_2$PbI$_4$ microplates at 78 K (Figure 1D).

To identify the origins of those two emission peaks, we carried out excitation-power-dependent PL studies at 78 K. As the excitation power increases, the intensity of both emission peaks increases (Figure 2A). We extracted the integrated emission intensity from Figure 2A and plotted against the excitation power as shown in Figure 2B. The power-dependent integrated emission intensity can be well fitted by a power function $I_{PL} \propto I_{ex}^{k}$, where I_{PL} stands for the integrated PL intensity, and I_{ex}, for the excitation power, and k is the fitting parameter. k values are 1.05 and 1.90 for those two emission peaks, respectively (Figure 2B) [26]. According to the fitting results and

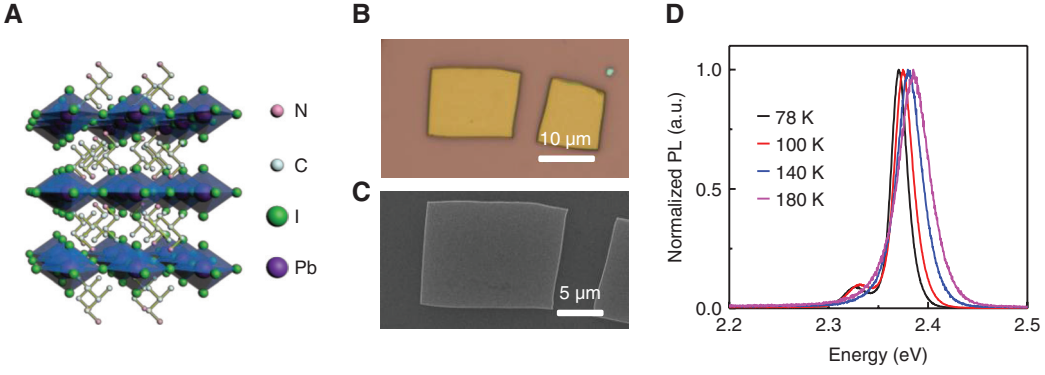

Figure 1: Crystal structure and PL spectra of (iso-BA)$_2$PbI$_4$ perovskite crystals.
(A) Crystal structure of (iso-BA)$_2$PbI$_4$. (B) The optical microscope image of the as-prepared (iso-BA)$_2$PbI$_4$ perovskite microplates. (C) The SEM image of (iso-BA)$_2$PbI$_4$ perovskite microplates. (D) The PL spectra of (iso-BA)$_2$PbI$_4$ perovskite microplate at different temperature.

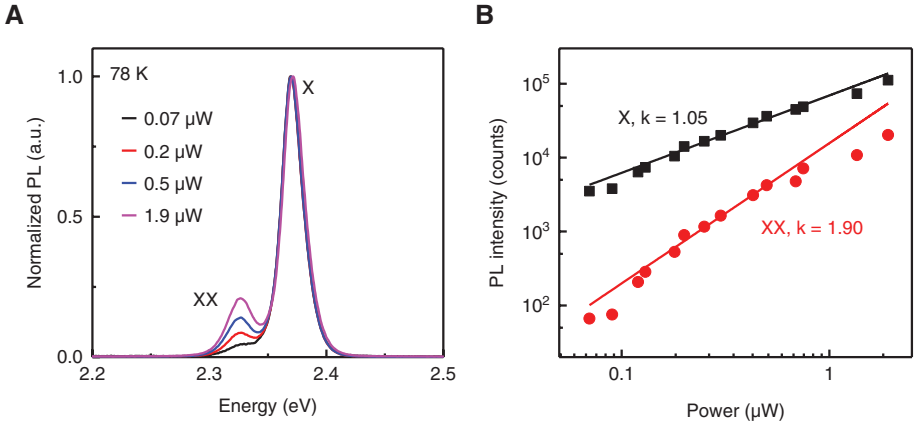

Figure 2: Power-dependent PL studies.
(A) Power-dependent PL spectra of a (iso-BA)$_2$PbI$_4$ perovskite microplate at 78 K under a 405-nm CW laser excitation. The thickness of the microplate is 60 nm, measured by atomic force microscope. (B) PL intensity vs. excitation power. The XX intensity obeys a power-law function of the excitation power ($I_{PL} \propto I_{ex}^{1.9}$).

temperature-dependent PL studies (Figure 1D), the two emission peaks can be assigned as free exciton (denoted as X) and biexciton emission (denoted as XX), respectively [27]. As the temperature increases, exciton emission intensity decreases (Figure S2) and the exciton emission peak gradually broadens (Figure 1D), resulting in the absence of the biexction emission at a higher temperature.

Strikingly, the biexciton emission peak can be clearly visualized when the excitation power is as low as 0.2 μW at 78 K for (iso-BA)$_2$PbI$_4$ microplate with a thickness of 60 nm, which corresponds to a power density of 6.4 W/cm^2 for a 405-nm continuous wavelength (CW) laser excitation. We also measured thickness-dependent biexcitons emissions, which are easily observed in thick samples due to the large density of excitons (Figure S3). The excitation power density of (iso-BA)$_2$PbI$_4$ excited by a CW laser is lower than that of other 2D materials (Table 1). The presence of biexciton emission under such low excitation power density can be ascribed to the high crystalline quality of the as-synthesized (iso-BA)$_2$PbI$_4$ crystals and multiple quantum well structure of (iso-BA)$_2$PbI$_4$ [28]. We have also carried out power- and temperature-dependent PL measurement for (n-BA)$_2$PbI$_4$ microplates and no biexciton emission was observed even under a higher excitation power due to different configurations of organic chains (Figure S4A and B).

From Figure 2A, the biexciton binding energy in (iso-BA)$_2$PbI$_4$ is estimated to be 46 meV, which is close to that in other 2D layered materials such as WSe_2 and comparable to that in 2D perovskites [11, 15]. This biexciton binding energy is approximately 20.8% of the corresponding exciton binding energy, which is extracted to be around 221 meV (Figure S5) [29].

To explain the large biexciton binding energy and the low excitation power density required to observe the biexciton emission, we propose that the biexciton possibly consists of a bright exciton and a dark exciton (denoted as D), the schematics of which is displayed in Figure 3. Under such configuration, the biexciton binding energy should be given by $\Delta_{XD} = E_X + E_D - E_{XD}$, where E_D is the energy of dark state, leading to the large biexciton binding energy, which has been proved in WSe_2 [9, 10].

Finally, the polarization-resolved PL spectra of (iso-BA)$_2$PbI$_4$ microplates at 78 K was conducted. The

Table 1: Summary of biexciton emission in 2D materials.

Material	Power	Temperature	Binding energy	Reference
WSe_2	1274 W/cm^2	4.2 K	16–17 meV	[10]
CdSe colloidal quantum wells	6.5 W/cm^2	Room temperature	30 ± 5 meV	[14]
(n-BA)$_2$PbBr$_4$	1 MW/cm^2	10 K	60 meV	[12]
$(C_{10}H_{21}NH_3)_2PbI_4$	100 kW/cm^2	2 K	50 meV	[13]
(iso-BA)$_2$PbI$_4$	6.4 W/cm^2	78 K	46 meV	This work

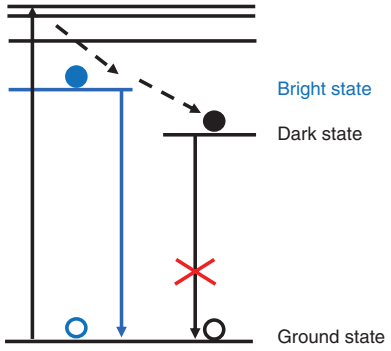

Figure 3: Possible dark exciton states in (iso-BA)$_2$PbI$_4$ perovskite.

schematic illustration of the measurement setup is displayed in Figure S6. Figure 4A shows two representative PL spectra under different detection polarization angles. It is obvious that both free exciton and biexciton emission depends on the detection polarization angle. We measured PL spectra by continuously tuning the detection polarization angle from 0° to 360° in a 10° step under an excitation power of 1.58 μW for the microplate with a thickness of 60 nm. The extracted integrated emission intensity vs. the detection polarization angle for both free exciton and biexciton emission is given in Figure 4B. Both curves can be well fitted by the function $I = I_0 \sin(2\theta + \varphi) + A$, where θ is the polarized angle. φ is the initial phase at the polarized angle of 0°. I_0 and A are the parameters for PL intensity and independent of polarization, respectively [22, 30]. The polarization orientation has a 90° difference between free exciton and biexction emission. We measured the polarization properties of (iso-BA)$_2$PbI$_4$ microplates with different thicknesses under an excitation power of 1.58 μW (Figure S7A and C). Figure S7B and D shows the polar plot of the emission intensity vs. polarization angle and they essentially exhibit similar anisotropy behavior for different thickness, indicating the thickness does not affect the polarization properties of the biexciton emission. The polarization properties of biexciton emission lines have been reported in semiconductor quantum dots (QDs) and quantum well crystal [2, 31]. In previous reports, the excitonic fine structure splitting and the polarization degree of the biexcitons are correlated in QD [32]. The exchange interaction is responsible for the splittings in different polarizations between excitons and biexcitons [33]. In this work, the emission peak position also exhibits a periodical shift with the detection polarization angle for both free exciton and biexciton emission (Figure 4C) but also has a 90° difference between free exciton and biexciton, similar to that of the intensity in Figure 4B. This 90° difference might be ascribed to the exchange splitting effect arising

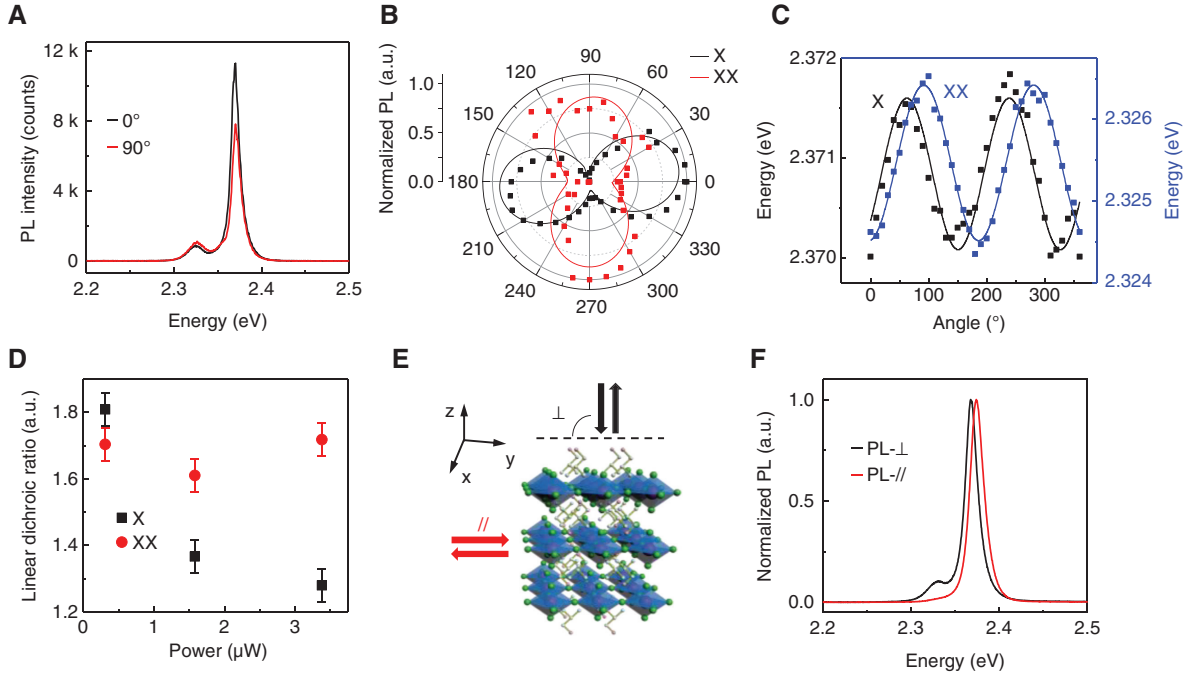

Figure 4: Polarization-resolved PL spectra for a microplate with a thickness of 60 nm.
(A) PL spectra at 78 K under different detection polarization angles. (B) Polarization resolved PL intensity for both exciton and biexciton emission under an excitation power of 1.58 μW. The solid lines are fitting results. (C) Polarization resolved PL emission energy for both exciton and biexciton emission under an excitation power of 1.58 μW. The solid lines are fitting results. (D) Linear dichroic ratios of excitons and biexcitons under different excitation power. (E, F) Schematic illustration (E) and PL spectra (F) from crystal plane and cross-section of a crystal plane under a 405-nm circularly polarized laser excitation at 78 K.

from the different configuration of free exciton and biexciton [34].

To characterize the emission anisotropy, the linear dichroic ratio was used, defined as the ratio of the maximum emission intensity to the minimum emission intensity [35]. Based on the fitting results, the linear dichroic ratios are estimated to be 1.28, 1.37 and 1.81 for free excitons and 1.72, 1.61 and 1.70 for biexcitons under excitation powers of 3.38 μW, 1.58 μW and 0.31 μW, respectively (Figure 4D). The larger linear dichroic ratio for biexcitons is probably due to the configuration of the biexcitons we proposed above. The opposite evolution of the linear dichroic ratio vs. the excitation power between the free excitons and the biexcitons suggests that the dark excitons might have a certain direction of polarization different from free excitons. Since the biexcitons tend to combine the two excitons in the in-plane direction, the dark excitons would also affect the anisotropy of the biexcitons. This is further supported by the PL emission from the crystal plane (PL-⊥) and the cross-section of the crystal (PL-//), as schematically illustrated in Figure 4E [36]. The weaker biexciton emission for PL-// compared to that for PL-⊥ (Figure 4F) suggests that biexcitons prefer to combine two excitons in the in-plane rather than out-of-plane, consistent with what we proposed above [37].

4 Conclusions

In summary, we have observed the biexciton emission in (iso-BA)$_2$PbI$_4$ perovskite microplates under a low excitation power density of 6.4 W/cm^2 at 78 K. The enhanced Coulomb interaction and the large nonlinear effect lead to the biexciton emission in (iso-BA)$_2$PbI$_4$ perovskite under such low excitation power density. The large biexciton binding energy of 46 meV for biexciton binding energy is approximately 20.8% of the exciton binding energy. The anisotropy of the biexcitons is different from that of the free excitons since the polarization direction of the biexcitons is more inclined to the crystalline plane. Our study is beneficial to the further understanding of biexcitons and has important applications of novel optoelectronics and biexciton lasing.

5 Supplementary materials

Supplementary figures (Figures S1–S7) and the corresponding discussion. This material is available from the author.

Acknowledgments: The authors acknowledge the support from NSFC (Funder Id: http://dx.doi.org/10.13039/501100001809, 61674060) and Innovation Fund of WNLO. They also thank the Testing Center of Huazhong University of Science and Technology for the support in thickness measurement.

References

[1] Krishna A, Gottis S, Nazeeruddin MK, Sauvage F. Mixed dimensional 2D/3D hybrid perovskite absorbers: the future of perovskite solar cells? Adv Funct Mater 2019;29:1806482.
[2] Tanaka K, Takahashi T, Kondo T, et al. Electronic and excitonic structures of inorganic-organic perovskite-type quantum-well crystal ($C_4H_9NH_3)_2PbBr_4$. Jpn J Appl Phys 2005;44:5923–32.
[3] Wang J, Su R, Xing J, et al. Room temperature coherently coupled exciton-polaritons in two-dimensional organic-inorganic perovskite. ACS Nano 2018;12:8382–9.
[4] Chen K, Wang Y, Liu J, et al. In situ preparation of a CsPbBr 3/black phosphorus heterostructure with an optimized interface and photodetector application. Nanoscale 2019;11:16852–9.
[5] Zhang Y, Lim C-K, Dai Z, et al. Photonics and optoelectronics using nano-structured hybrid perovskite media and their optical cavities. Phys Rep 2019;795:1–51.
[6] Wu L, Chen K, Huang W, et al. Perovskite CsPbX3: a promising nonlinear optical material and its applications for ambient all-optical switching with enhanced stability. Adv Opt Mater 2018;6:1800400.
[7] Li J, Wang J, Ma J, et al. Self-trapped state enabled filterless narrowband photodetections in 2D layered perovskite single crystals. Nat Commun 2019;10:806.
[8] Qi X, Zhang Y, Ou Q, et al. Photonics and optoelectronics of 2D metal-halide perovskites. Small 2018;31:1800682.
[9] Chen SY, Goldstein T, Taniguchi T, Watanabe K, Yan J. Coulomb-bound four-and five-particle intervalley states in an atomically-thin semiconductor. Nat Commun 2018;9:3717.
[10] Li Z, Wang T, Lu Z, et al. Revealing the biexciton and trion-exciton complexes in BN encapsulated WSe_2. Nat Commun 2018;9:3719.
[11] You Y, Zhang XX, Berkelbach TC, Hybertsen MS, Reichman DR, Heinz TF. Observation of biexcitons in monolayer WSe_2. Nat Phys 2015;11:477–81.
[12] Kato Y, Ichii D, Ohashi K, et al. Extremely large binding energy of biexcitons in an organic-inorganic quantum-well material ($C_4H_9NH_3)_2PbBr_4$. Solid State Commun 2003;128:15–8.
[13] Ishihara T, Hong X, Ding J, Nurmikko A. Dielectric confinement effect for exciton and biexciton states in PbI_4-based two-dimensional semiconductor structures. Surf Sci 1992;267:323–6.
[14] Grim JQ, Christodoulou S, Di Stasio F, et al. Continuous-wave biexciton lasing at room temperature using solution-processed quantum wells. Nat Nanotechnol 2014;9:891–5.
[15] Thouin F, Neutzner S, Cortecchia D, et al. Stable biexcitons in two-dimensional metal-halide perovskites with strong dynamic lattice disorder. Phys Rev Mater 2018;2:034001.
[16] Booker EP, Price MB, Budden PJ, et al. Vertical cavity biexciton lasing in 2D dodecylammonium lead iodide perovskites. Adv Opt Mater 2018;6:1800616.

[17] Chen Y, Sun Y, Peng J, Tang J, Zheng K, Liang Z. 2D Ruddlesden-Popper perovskites for optoelectronics. Adv Mater 2018;30:1703487.
[18] Li C, Liu Z, Chen J, Gao Y, Li M, Zhang Q. Semiconductor nanowire plasmonic lasers. Nanophotonics 2019;8:2091–110.
[19] Chen K, Zhong Q, Chen W, et al. Short-chain ligand-passivated stable α-CsPbI$_3$ quantum dot for all-inorganic perovskite solar cells. Adv Funct Mater 2019;29:1900991.
[20] Liu J, Shabbir B, Wang C, et al. Flexible, printable soft-X-ray detectors based on all-inorganic perovskite quantum dots. Adv Mater 2019;31:1901644.
[21] Wang J, Li J, Tan Q, et al. Controllable synthesis of two-dimensional Ruddlesden-Popper-type perovskite heterostructures. J Phys Chem Lett 2017;8:6211–9.
[22] Li L, Jin L, Zhou Y, et al. Filterless polarization-sensitive 2D perovskite narrowband photodetectors. Adv Opt Mater 2019;7:1900988.
[23] Chen Y, Sun Y, Peng J, et al. Tailoring organic cation of 2D air-stable organometal halide perovskites for highly efficient planar solar cells. Adv Energy Mater 2017;7:1700162.
[24] Etgar L. The merit of perovskite's dimensionality; can this replace the 3D halide perovskite? Energy Environ Sci 2018;11:234–42.
[25] Stoumpos CC, Cao DH, Clark DJ, et al. Ruddlesden-Popper hybrid lead iodide perovskite 2D homologous semiconductors. Chem Mater 2016;28:2852–67.
[26] Li W, Fang C, Wang H, et al. Surface depletion field in 2D perovskite microplates: structural phase transition, quantum confinement and Stark effect. Nano Res 2019;12:2858–65.
[27] Makino H, Goto T, Yao T, Mousdis GA, Papavassiliou GC. Induced absorption and spontaneous emission due to biexciton in two-dimensional semiconductor $(CH_3C_6H_4CH_2NH_3)_2PbBr_4$ single crystal. J Lumin 2005;112:54–7.
[28] Woggon U, Hild K, Gindele F, et al. Huge binding energy of localized biexcitons in CdS/ZnS quantum structures. Phys Rev B 2000;61:12632–5.
[29] Blancon JC, Stier AV, Tsai H, et al. Scaling law for excitons in 2D perovskite quantum wells. Nat Commun 2018;9:2254.
[30] Wang X, Li Y, Huang L, et al. Short-wave near-infrared linear dichroism of two-dimensional germanium selenide. J Am Chem Soc 2017;139:14976–82.
[31] Reischle M, Beirne G, Roßbach R, Jetter M, Michler P. Influence of the dark exciton state on the optical and quantum optical properties of single quantum dots. Phys Rev Lett 2008;101:146402.
[32] Bayer M, Ortner G, Stern O, et al. Fine structure of neutral and charged excitons in self-assembled In(Ga)As/(Al)GaAs quantum dots. Phys Rev B 2002;65:195315.
[33] Amloy S, Chen Y, Karlsson K, et al. Polarization-resolved fine-structure splitting of zero-dimensional $In_xGa_{1-x}N$ excitons. Phys Rev B 2011;83:201307.
[34] Shang J, Shen X, Cong C, et al. Observation of excitonic fine structure in a 2D transition-metal dichalcogenide semiconductor. ACS Nano 2015;9:647–55.
[35] Song Q, Wang H, Pan X, et al. Anomalous in-plane anisotropic Raman response of monoclinic semimetal 1 T-$MoTe_2$. Sci Rep 2017;7:1758.
[36] Sheikh T, Shinde A, Mahamuni S, Nag A. Possible dual bandgap in $(C_4H_9NH_3)_2PbI_4$ 2D layered perovskite: single-crystal and exfoliated few-layer. ACS Energy Lett 2018;3:2940–6.
[37] Musia A, Sęk G, Misiewicz J, et al. Effect of Confinement anisotropy on excitonic properties in InAs/InP quantum dashes. Acta Phys Pol A 2013;124:801–4.

Supplementary Material: The online version of this article offers supplementary material (https://doi.org/10.1515/nanoph-2019-0528).